Cubic to Cylindrical Transition in Diblock Copolymers Induced by Strain

G. G. Pereira*

Department of Mechanical Engineering, University of Sydney, Sydney, 2006 Australia

Received January 22, 2003; Revised Manuscript Received November 14, 2003

ABSTRACT: I consider the problem of a body centered cubic (bcc), spherical meso-structure subjected to a uniform strain. Such a phase occurs for diblock copolymer melts when the fraction of the minority block, *f*, is roughly between 0.05 and 0.12. I determine how the spherical structure distorts when a strain is applied and find that the deformation is ellipsoidal. I then calculate the free energy cost of such a deformation and the bulk deformation constants i.e., elastic modulii. I also consider the stability of the deformed spherical morphology (ellipsoids) vs a cylindrical morphology and the approximate change in the phase boundary between the two morphologies as a function of strain. I consider how one may use this method, together with an applied electric field, to induce a cylindrical morphology from an initial bcc melt. If this were possible, this process would offer one avenue to reduce the radius of the cylinders, below the limit of the bulk cylindrical phase. This could lead to the possibility of nanowires with smaller radii.

1. Introduction

Much effort recently has been devoted to miniaturization of devices from the micrometer-scale range to the nanoscale regime. The application of such devices has some obvious advantages, including drastically increased speeds and capacities. One route to descend into the nano regime has been to utilize the inherent property of certain materials to self-assemble or self-organize into regular, crystal patterns. One example of such a material is a block copolymer melt. Block copolymers consist of at least two chemically different polymer chains tethered together. It has been seen[1] that a wide variety of beautiful and complicated patterns (or morphologies) may result from the self-assembly of such melts. The length scale on which these periodical patterns replicate themselves is related to the number of monomers per chain and, consequently, is on the order of 10−100 nm.

In outlining the possible technological applications of these block copolymer melts, I have not mentioned the many obstacles which are involved in obtaining the regular crystal patterns. For example, although these patterns are predicted theoretically to be stable states, experimentally one often finds that, on a global scale, the patterns are disrupted by defects or grain boundaries where the different grains do not match up. That is, locally the patterns do form, but on a global scale, i.e., micrometers to millimeters, there is a lack of order. In overcoming this problem, it has been suggested that one confines the block copolymer melt to a thin film. Subsequently, external fields are applied in an attempt to iron out the defects. These confined systems are of considerable scientific interest themselves because, besides the bulk behavior of the melt, one must also consider confinement effects due to the bounding surfaces.

Although there are a wide variety of block copolymer architectures, I shall focus on the simplest architecture—that of linear, diblock copolymers. Diblock copolymers are made up of two chemically different polymer chains, denoted by A and B, joined together end to end. The self-assembly of the diblocks is driven by the immiscibility of the A and B components, leading to microphase separation into a variety of morphologies with a characteristic size of order 100 nm. Some typical morphologies that form are lamellae, cylindrical and spherical phases.[2] Here I concentrate on the case of an asymmetric diblock melt which forms a body centered cubic (bcc) packed, spherical phase in the bulk. This has been shown to form (and seen experimentally) at a fraction of A monomers, denoted by *f*, between[2] 0.05 and 0.12. I consider chains with degree of polymerization *N*, and identical monomer size *a*. This morphology minimizes the sum of AB interfacial energy and elastic stretching energy of the chains.

Much work in the past has focused on thin films of the lamella phase[3,4] and recently work has been initiated on thin film melts of the cylindrical phase.[5−11] Work on thin film melts of the bcc phase of diblocks is sparser. In this paper, I therefore turn my attention to this problem. Note that very recently a few papers have appeared which deal with some aspects of the bcc phase[12−14] considered here. These papers, although related to the work in my research group, have a different emphasis.

When a block copolymer melt is confined to a thin film of thickness *D*, the block copolymer morphology may be under an external strain. The reason is the following: The bcc phase of diblocks has a certain (equilibrium) center-to-center sphere spacing. Let us call this spacing D_0. Now since *D* can, in principle, vary continuously it will not always be some integral multiple of D_0. As a result an external strain is applied to the spherical geometry and consequently on the block copolymer system. Since the block copolymer melt is incompressible, if there is a fixed amount of chains present (i.e., by fixing the volume of the sample), the melt would have to conserve volume under the imposition of an external strain by either contraction or elongating appropriately in the two orthogonal directions to the strain. However, I envisage a slightly different scenario here. The melt sample is connected to an infinite reservoir of chains. Thus, as the sample thickness varies (for example as *D* increases) as many chains as is required will enter the

10.1021/ma030052j CCC: $27.50
Published on Web 01/21/2004

sample from the reservoir and fill the available volume. Hence the melt incompressibility is conserved.

I shall give a mathematical definition of the external strain in section 2. How the bcc melt responds to this external strain is one of the essential questions in this paper. It may respond either by deforming the spherical minority domains in an isotropic manner (i.e., either by dilating or shrinking the spheres) so that the spherical shape is preserved. On the other hand, the deformation may be anisotropic (i.e., the shape of the spheres deform to an ellipsoidal shape). The first deformation, in response to an imposed strain, I shall refer to as an *isotropic deformation*, and the second deformation, I shall refer to as an *anisotropic deformation*. (Very recently, after this manuscript was submitted, I was made aware of the paper by Tyler and Morse,[12] which evaluates elastic modulii for a bcc melt of diblocks via self-consistent field theory. Their emphasis is on the experimental, from rheological data, and numerical comparison of the elastic modulii. Besides working in the strong segregation regime, my emphasis is on the thin film properties of the bcc phase. My work and Tyler and Morse's[12] work should therefore be seen as complementary to each other.)

I shall therefore answer the question posed above, which in truth, can also be applied to bulk melt samples. Thus, another important contribution of this paper is the determination of the bulk modulii of elasticity of the bcc phase. (For example, external strains can be applied to bulk melts by shear or elongational stress fields, or simply by a slight mismatch between the lattice constant D_0 and sample size D. In bulk melts, however, D would be very large, so the strain would always be very small.) It will be observed that the free energy of an anisotropic deformation is less that an isotropic deformation, so I predict the spheres to form ellipsoids under an external strain. It will also be seen that under sufficiently large strains the bcc phase may become unstable in comparison to the cylindrical phase, for minority block fractions below 0.12. I then proceed to the thin film problem and determine under what conditions the deformed bcc phase will be stable and under what conditions the cylindrical phase will be stable. This naturally leads us to a very recent application for these block copolymer melts in the formation of nanowires.[15,16] These are wires (of circular cross-section) whose radii are on the order of nanometers. Because the cylindrical phase exists for minority block fractions above about 0.12, there is a limit to how small the radii of the nanowires can be. In this context, I consider using the bcc phase as a starting point and then attempt to transform this phase into the cylindrical phase. This is done with a combination of application of external strain and an electric field perpendicular to the confining surfaces.

2. Free Energy

I shall concentrate the theoretical analysis on the strong segregation limit[17,18] (SSL), where the interfacial tension between the different blocks becomes infinitely large. One commonly refers to this limit as $\chi N \rightarrow \infty$ where χ is the Flory−Huggins parameter, which measures the incompatability between the A and B monomer types. In this limit, the bcc phase is expected to occur below $f \approx 0.12$. The free energy for curved geometries is approximate. I therefore consider upper and lower bounds to the actual energy. The unit cell approximation (UCA) gives a lower bound to the actual free energy since I assume the boundary of the Wigner−Seitz cell is a sphere, whereas in reality this geometry would not completely fill space. To completely fill space, extra chains would need to be added which would result in a net increase in the free energy. On the other hand, I could use a Wigner−Seitz cell which completely packs space, i.e., a cell appropriate for a bcc cubic lattice (Figure 1). Then the Straight Paths Approximation (SPA) with a nonround unit cell gives an upper bound to the actual free energy, because now the AB interface is assumed to be the same shape as the outer boundary of the Wigner−Seitz cell, although scaled down. In reality, the AB interface is much smoother (and rounder) and so the SPA gives an upper bound to the actual energy.

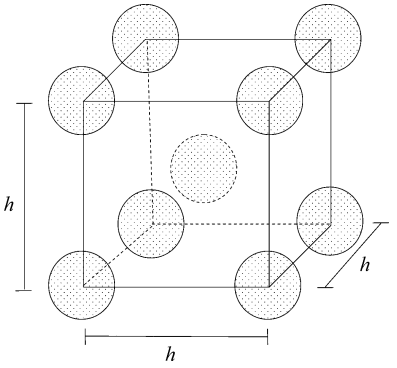

Figure 1. Schematic for the bcc morphology. The centers of the spheres, which represent the AB dividing surfaces, are located at the vertexes of the cube and one sphere is at the center of the cube. The cube side length is h.

For a bcc crystal there are three different modulii of elasticity (or elastic constants) to consider. The first one is due to bulk dilation (or shrinkage) caused by an isotropic change in the crystal domain spacing. The elastic constant for this deformation is determined (via both UCA and SPA) in sections 2.1.1 and 2.2.1 and denoted $\bar{B}$ (following de Gennes' notation in ref 19). The second modulus is an elongation in the [100] crystal axis direction (see Figure 1). I shall evaluate this constant in sections 2.1.2 and 2.2.2, and it is denoted C. There is a third elastic modulus which corresponds to elongation in the [111] crystal direction (Figure 1). This constant can only be determined in the SPA; in the UCA the [100] and [111] crystal axes are indistinguishable. However, in this paper I do not evaluate it, for one major reason. As we shall see, the SPA calculations are arduous to say the least. Since the real aim of this paper is to work out thin film free energies, rather than elastic modulii, I feel the extra work involved in calculating this constant is not warranted. Tyler and Morse[12] have very recently shown that this modulus is slightly greater than C, from self-consistent field calculations. In my thin film results I shall assume that the modulus for the [111] deformation is the same as C. As far as the UCA calculation is concerned such an assumption is not necessary.

2.1. Free Energy via UCA. 2.1.1. Isotropic (UCA) Case. Consider first the free energy for the bcc spherical phase of diblock copolymers calculated via the unit cell approximation (UCA). I initially show how the free energy for the spherically symmetric case (isotropic system) is calculated, as a lead into the more complicated ellipsoidal case (anisotropic system). The free energy consists of the AB interfacial energy, F_{AB}, and

the elastic, stretching energy, F_{el}, which derives from the chain entropy. I divide the sphere into wedges of radius R which subtend longitudinal and latitudinal angles $\delta\theta$ and $\delta\phi$, respectively. Then the surface energy in the SSL, of a typical wedge, is just $\gamma_{AB}\beta^2 A_{wedge}$ where A_{wedge} is the surface area of the wedge and $\beta = f^{1/3}$ in the bcc case. I therefore obtain the surface energy of a typical wedge as $\gamma_{AB}f^{2/3}R^2 \sin\theta\delta\theta\delta\phi$. To obtain the total surface energy between A and B domains I sum this quantity over the entire sphere so that $F_{AB} = \gamma_{AB}f^{2/3}\sum_{wedges}R^2 \sin\theta\delta\theta\delta\phi$. The elastic energy of each wedge is, according to Olmsted and Milner[18]

$$F_{el,wedge} = \frac{k_B T}{8Nv}\frac{\pi^2}{6Na^2}\left[\frac{I_A}{f^2} + \frac{I_B}{(1-f)^2}\right]R^3 A_{wedge} \quad (1)$$

where I_A and I_B are derived from the monomer chemical potentials in the A and B domains. According to Olmsted and Milner, they are given by

$$I_A = 3\int_0^{\beta}(\beta - y)^2 y^2\, dy \quad \text{and} \quad I_B = 3\int_0^{1-\beta}(\beta + y)^2 y^2\, dy \quad (2)$$

I_A and I_B are given by $I_A = f^{5/3}/10$ and $I_B = (1 - f^{1/3})^3(f^{2/3} + 3f^{1/3} + 6)/10$. This elastic energy is summed, just as the interfacial energy, over the whole sphere. I now have the total energy of an AB spherical Wigner−Seitz cell. To obtain the free energy per chain, I divide this quantity by the number of chains, which is just $\sum_{wedges}(R^3/3)\sin\theta\delta\theta\delta\phi/(Nv)$. The sums can be easily evaluated in the limit of $\delta\theta, \delta\phi \to 0$, so that I get the free energy per chain F_{uca} in the UCA, of the spherical phase to be $F_{uca} = \square/R + \bigcirc R^2$ where

$$\square = 3\gamma_{AB}f^{2/3}Nv \quad \text{and}$$
$$\bigcirc = \frac{k_B T\pi^2}{16Na^2}\left[\frac{1}{10f^{1/3}} + \frac{(1-f^{1/3})^3(f^{2/3}+3f^{1/3}+6)}{10(1-f)^2}\right] \quad (3)$$

Minimizing F_{uca} over R one finds the optimal radius is $R_{opt} = (\square/2\bigcirc)^{1/3}$ and the minimum free energy, per chain, is F_0 given by

$$F_0 = \frac{3\square^{2/3}\bigcirc^{1/3}}{2^{2/3}} = 3k_B T\left(\frac{27\pi^2}{96}\right)^{1/3}\left(\frac{\gamma_{AB}a^2}{k_B T}\right)^{2/3}\left(\frac{v^{1/3}}{a}\right)^2\frac{N^{1/3}}{20^{1/3}} \times \left[f + \frac{f^{4/3}(1-f^{1/3})^3(f^{2/3}+3f^{1/3}+6)}{(1-f)^2}\right]^{1/3} \quad (4)$$

I now turn to the case when a strain is applied to the bulk bcc spherical phase. This can occur, for example, when the bulk melt is confined to a thin film geometry. I want to determine what shape the spherical domains will take up under either a positive (elongation) or negative (compression) strain. Initially consider the simplest scenario: The sphere radius just gets larger (under elongation) or smaller (under compression). This I refer to as bulk dilation. Thus, I introduce the uniform strain $\epsilon \equiv R/R_{opt} - 1$. It is positive when the system is elongated, negative when compressed and zero at equilibrium. (For notational convenience I also shall define and use $\lambda \equiv R/R_{opt} = \epsilon + 1$.) In bulk dilation the free energy only depends on λ. I may rewrite F_{uca}, using (4), as

$$F_{uca} = \frac{2}{3}F_0\lambda^{-1} + \frac{1}{3}F_0\lambda^2 \quad (5)$$

Thus, the bulk dilation constant $\bar{B}$ is $\bar{B} = (d^2F_{uca}/d\lambda^2)_{\lambda=1}$ giving $\bar{B} = 2F_0$.

In the following calculations, I always calculate the free energy, per chain, of a typical Wigner−Seitz cell in the following manner. I allow a particular strain (λ) along one of the axes of my Wigner−Seitz cell. I assume an affine deformation where the inner domain and outer domain deform in the same manner (see below). The free energy of the cell is calculated (via the wedge method). The number of chains in the cell is also calculated by simply dividing the cell's volume by the volume of one chain. Hence the free energy per chain is calculated for any possible geometry. This free energy per chain is then minimized (for a particular strain) over all possible geometrical shapes. In doing this I do not constrain the dimensions of the Wigner−Seitz cell in the two orthogonal directions (to the imposed strain) but instead let them relax to their optimum values.

2.1.2. Anisotropic (UCA) Case. Besides the simplest scenario described above, the other obvious distortion is that the spheres deform anisotropically into ellipsoidal shapes. I shall assume an affine deformation of the spheres; i.e., the inner and outer ellipsoids have the same shape and their dimensions are related by the factor $f^{1/3}$. The ellipsoid has the equation $x^2/l_x^2 + y^2/l_y^2 + z^2 = R^2$. Initially, I shall determine whether, under a strain, the system deforms so that $l_x = l_y$ (i.e., isotropically in the orthogonal directions). On physical grounds one would assume that this would be the case. In Appendix A, I determine the radius and typical differential area element for the ellipsoid in polar coordinates. I also show how to evaluate the ellipsoidal configuration's free energy as a function of R, l_x, and l_y. One can minimize the energy for a particular strain (i.e., particular λ) and determine whether the optimal orthogonal relaxations are such that $l_x = l_y$. This, in fact, is a computationally expensive task so I just evaluate the energy for a few particular strains to see whether my assumption is validated. The energy is a function of $\beta \equiv 1 - (l_y/l_x)^2$ and $l \equiv l_y$. For example, at a strain of $\lambda = 1.1$ I find the optimal β is zero and $l = 0.9097$, while for a strain of $\lambda = 0.9$ I find the optimal β is zero and $l = 1.096899$.

Thus, we have seen when a strain is applied to the system, the deformations in the two orthogonal directions to the imposed strain are exactly the same. This makes physical sense since there is no preferred direction in the plane orthogonal to the imposed strain for the system to relax. Thus, if the system is elongating, the ellipsoid will be a prolate spheroid, while if it is being compressed, it will be an oblate spheroid. Let the strain be applied in the z direction and so the equation of the ellipsoid in Cartesian cordinates is $(x^2 + y^2)/l^2 + z^2 = R^2$ and in polar coordinates is

$$r(\theta,\phi) = R(1-e^2)^{1/2}(1 - e^2\cos^2\phi)^{-1/2} \quad \text{or}$$
$$r(\theta,\phi) = R(1-e^2)^{-1/2}\left(1 + \frac{e^2}{1-e^2}\cos^2\phi\right)^{-1/2} \quad (6)$$

for the prolate and oblate spheroids, respectively. Here, l and the eccentricity e are related by $e^2 = 1 - l^2$ for a prolate spheroid, and $e^2 = 1 - l^{-2}$ for an oblate spheroid. I have given the radius function for the deformed geometry. At this point I can launch into the free energy calculation. This, however, is quite tedious and detracts from the physical results. So I shall complete the calculation in Appendix B. Here I just give the results.

The total free energy per chain of the ellipsoid is $F_{uca} = (F_{AB} + F_{el})/(V/Nv)$. After some rearrangement (and completing the integrals) I obtain the convenient form

$$F_{uca}(\lambda, e^2) = \frac{2}{3}F_0\lambda^{-1}\frac{1}{2}[1 + (1 - e^2)^{-1/2}e^{-1}\arcsin(e)] + \frac{1}{3}F_0\lambda^2\left[1 - \frac{2e^2}{3}\right] \quad (7)$$

The elliptic deformation constant, C, is given by $C \equiv [(\partial^2 F_{uca}/\partial(e^2)^2)]_{e^2=0,\lambda=1}$. The first derivative gives zero, as required, since I am expanding about a minima. Evaluating the second derivative gives $C = 16F_0/45$, within the UCA.

In the oblate spheroid case, I find the total free energy per chain is

$$F_{uca}(\lambda, e^2) = \frac{2}{3}F_0\lambda^{-1}\frac{1}{2}\left[1 + \frac{(1 - e^2)}{2e}\ln\left(\frac{1 + e}{1 - e}\right)\right] + \frac{1}{3}F_0\lambda^2\left[\frac{3 - e^2}{3(1 - e^2)}\right] \quad (8)$$

The elliptic deformation constant, C, is given by $C = 16F_0/45$, within UCA. Note that the prolate deformation constant is equal to the oblate deformation constant, which is a result of the relaxations in the two orthogonal directions to the imposed strain being the same. Also, if I compare these constants with the bulk dilational constant, $\bar{B}$, I find they are much smaller. For a particular strain in the system, λ, the free energy should be minimized over the eccentricity to obtain the optimal relaxation in the orthogonal directions and hence, the minimum free energy.

2.2. Free Energy via SPA. 2.2.1. Isotropic (SPA) Case. First I consider the free energy in the isotropic case. In the SPA the Wigner−Seitz cell boundary consists of 6 square faces which form on the faces of the cube and eight hexagonal faces which form on the corners.[20] The side length of the cube on which the Wigner−Seitz cell is based is h. Obtaining results for the isotropic SPA case is tedious and detracts from the physical description. Thus, I relegate the discussion on this calculation to Appendix C. Here I merely state the result.

The total free energy per chain is $F_{spa} = (\square/(h/2))(^1/_2 + \sqrt{3})^1/_2 + \bigcirc((h/2))^2(1561/5760 + 697/960)$. Minimizing this energy with respect to h one finds the optimal h is given by $(h/2)_{opt} = R_{opt}[(^1/_2 + \sqrt{3})/(5743/2880)]^{1/3}$ and the minimum free energy,[21] $\bar{F}_{spa}$, is $\bar{F}_{spa} = F_0(^1/_2 + \sqrt{3})^{2/3}(5743/23040)^{1/3}$.

Once again in the case of a strain applied to the bulk bcc phase, one may have either bulk (isotropic) dilation or an anisotropic deformation. In the former case, one may write the free energy as

$$F_{spa} = \frac{2}{3}\bar{F}_{spa}\lambda^{-1} + \frac{1}{3}\bar{F}_{spa}\lambda^2 \quad (9)$$

and so the bulk dilational constant $\bar{B}$ is $\bar{B} = (d^2F_{spa}/d\lambda^2)_{\lambda=1}$ giving $\bar{B} = 2\bar{F}_{spa}$.

2.2.2. Anisotropic (SPA) Case. When the bcc phase deforms anisotropically, in the SPA, the square faces on the sides of the cube which are parallel to strain direction are no longer square but become rhombuses. The (isotropic) hexagonal faces become longer in one direction than the other directions. The square faces on cube sides which are perpendicular to the strain direction will remain square in shape as the geometry should be isotropic in this direction (see Figure 2). Therefore, the free energy calculation can be divided into three parts: (i) the elongated rhombus faces (of which there are two such faces), (ii) the anisotropic slanted hexagonal face and (iii) the isotropic square face. I assume the cube deforms to a rectangular parallelepipid or cuboid. The cuboid has length h in the direction of strain and the other two sides are of length lh. Once again, obtaining results in this case is tedious and so I relegate discussion of this to Appendix D. Here I just give the result.

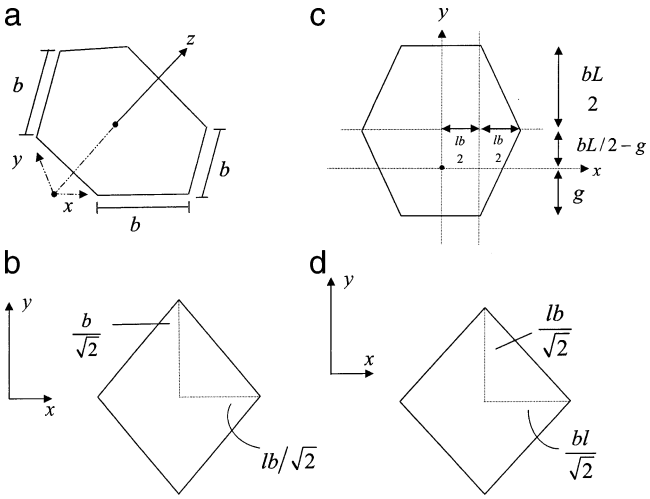

Figure 2. Schematic for the SPA calculations. (a) Isotropic case for the slanted hexagonal face. I define the z-axis to be perpendicular to the face with the origin of the Cartesian axes at the center of the Wigner−Seitz cell. The x and y axes then lie in a plane which is parallel to the plane of the hexagonal face. (b) Anisotropic case: rhombus face which is parallel to strain direction. (c) Anisotropic case: hexagonal, slanted face. I define the z-axis to be perpendicular to the slanted face and the origin is at the center of the Wigner−Seitz cell. The z axis goes through a point g units from the bottom of one edge. (d) Anisotropic case: rhombus face which is perpendicular to strain direction.

The free energy for an anisotropic deformation within the SPA is

$$F_{spa}(\lambda, l) = \frac{2}{3}\bar{F}_{spa}\lambda^{-1}J_1(l) + \frac{1}{3}\bar{F}_{spa}\lambda^2 J_2(l) \quad (10)$$

where $J_1(l) = (2l + 6Ll + l^2)/[3l^2(1 + 2\sqrt{3})]$ and $J_2(l) = (3840/5743l^2)(2I_i + I_{ii} + I_{iii})$. Note, $J_1(1) = 1$ and $J_2(1) = 1$.

I can evaluate the elliptic deformation constant, C, which is given in the SPA by

$$C \equiv \left[\frac{\partial^2 F_{spa}}{\partial l^2}\right]_{\lambda=1,l=1}\left[\frac{dl}{d(e^2)}\right]^2_{e^2=0}$$

Doing this, and after some algebra, I find $C = {}^1/_9[(10/\sqrt{3}(1 + 2\sqrt{3})) + 6373/5743]\bar{F}_{spa} \approx 0.41\bar{F}_{spa} \approx 0.44F_0$. (Recall, from UCA I get $C \approx 0.35F_0$.) Once again, as with the UCA, the elliptic deformation constant is much smaller than the bulk dilational constant.

At this point it is possible to make a comparison between my SSL elastic modulii (for $\chi N \rightarrow \infty$) and the self-consistent mean field modulii from Tyler and Morse[12] which are calculated at $\chi N \approx 19$. The most important point to note about the comparison is that they are at widely different degrees of segregation and so, as far

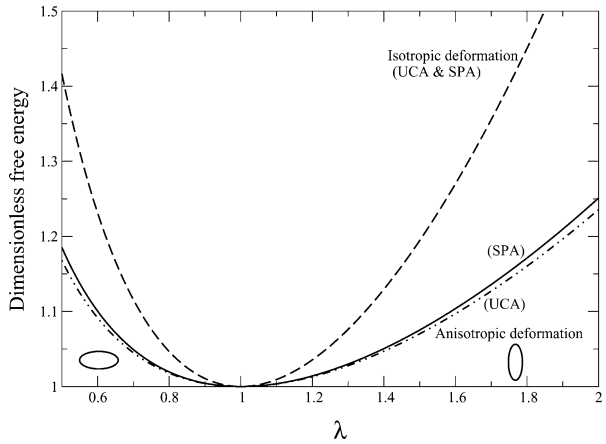

Figure 3. Dimensionless free energy (F/F_0 for the UCA calculations and $F/\bar{F}_{spa}$ for the SPA calculations) vs strain, λ. The isotropic deformation (dilation) is the dashed curve, the anisotropic SPA calculation is the filled bold curve and the dot−dashed curve is the anisotropic UCA calculation.

as quantitative comparison is concerned, the differences may not be too surprising. With this in mind, I find from the SSL calculation that the ratio $\bar{B}/C \approx 4.5$. From Tyler and Morse (using their Figure 3), I obtain $\bar{B}/C \approx 1.23$.[26] Further SCF calcuations, at much higher χN's, have to be done to see if such a difference truly exists or is rather just a result of the widely different χN's sampled.

3. Morphology of the Bcc Phase Under Strain

I have evaluated the free energies of the spherical phase under an imposed strain in the previous section. The energies, although approximate, give upper (SPA) and lower (UCA) bounds of the actual energy for this phase, for the isotropic deformation and estimates of this energy for the anisotropic deformation. It is important to note that a more precise evaluation of the bcc phase free energy, in the SSL, using analytic methods such as Semenov[17] and Olmsted and Milner,[18] is extremely difficult since the exact geometry of the AB interface is not as simple as the surface of a sphere. In fact, there are small perturbations to this geometry, as has been discussed before.[22] For example, if one were to use a spherical AB interface and the nonround, space filling bcc Wigner−Seitz cell, one would not be able to obtain an estimate of the elliptic constant C, as given in the previous section. Instead, the free energy would not have a global minima at[7−9,11] $\lambda = 1$, indicating such a geometry is not the minimum free energy state. I emphasize this point because, although it seems of minor importance, it is in fact the reason I have elected to calculate the free energy via two different methods to obtain estimates. We shall see below that the results are independent of which method (i.e., either UCA or SPA) I use. These estimates suggest that when the bcc phase is put under strain, the central spherical cores will deform to ellipsoids.

First, I consider the free energy of the bcc phase under a uniform strain. In Figure 3 I plot the dimensionless free energy vs strain, λ, for both the isotropic deformation, i.e., spheres with varying radii and an anisotropic deformation, i.e., an ellipsoidal geometry. In all cases I scale the free energies with their respective unstrained (equilibrium) energies—F_0 for UCA calculations and $\bar{F}_{spa}$ for SPA calculations. It is clear that an anisotropic deformation occurs at much lower free energy cost than an isotropic deformation. This is in agreement with my deformation constants $\bar{B}$ and C calculated in the previous section and valid at $\lambda \rightarrow 1$. Thus, when the bcc phase of a diblock melt is placed under a strain, the spherical domains will deform anisotropically. If put under compression, the spherical domain will deform to an oblate spheroid while, if put under elongation, it will deform to a prolate spheroid.

Under strain I have seen the spherical phase will deform anisotropically so that the spheres become ellipsoids. However, if the strain is significantly different from unity, there is another option the melt may take, i.e., a cylindrical morphology can result with the cylinder axes forming parallel to the direction of strain. In this orientation, the cylinders, in fact, pay no energy penalty as the strain in the system increases. Thus, a new morphology results, induced by strain. This is in contrast to the case when either the cylindrical or lamellar phase is put under strain. In these cases, a new morphology will not result because the melt may reorient itself so that chains line up such that they are orthogonal to the strain direction. That is, the cylinders align such that their long axis aligns with the strain direction or the lamellae align such that the sheets are parallel to the strain direction. The bcc phase, being symmetric in the three axial directions, has no such possibility and therefore when reorienting cannot completely compensate for the imposed strain.

To determine when and where each morphology exists under strain, I need the free energy of the cylindrical phase. The cylindrical phase free energy can also be determined via the wedge method.[15] In the UCA the cylindrical phase free energy, G_{uca} is

$$G_{uca} = k_B T \left(\frac{27\pi^2}{96}\right)^{1/3} \left(\frac{\gamma_{AB} a^2}{k_B T}\right)^{2/3} \left(\frac{v^{1/3}}{a}\right)^2 N^{1/3} \times \left[f + \frac{f(1-f^{1/2})^3(3+f^{1/2})}{(1-f)^2}\right]^{1/3} \quad (11)$$

Disregarding the f dependence in the spherical phase free energy and cylindrical phase free energy, these two phases free energies then only differ by a factor of $3/20^{1/3}$. In the SPA the cylindrical phase free energy is G_{spa} and $G_{spa} = (10/9)^{1/3} G_{uca}$. Within the UCA, the fraction f of minority block, at which there is a phase transition from the cylindrical phase to bcc phase is approximately 0.117, while in this SPA approximation this is much lower at around 0.056.

In Figure 4, I plot the free energy of the bcc phase and also the cylindrical phase for a fraction of minority phase of $f = 0.10$ and $f = 0.05$ using the UCA. (The results using the SPA are identical with the exception that the fraction f for the minority block has to be much lower. Thus, I do not show it here.) Note that the free energies are scaled with the equilibrium energy of the bcc phase F_0, at that particular f, so that only the cylindrical phase energy appears to change. One sees that at $f = 0.1$, for $\lambda > 1.16$ or $\lambda < 0.86$, the cylindrical phase becomes preferable, while at the lower f of 0.05, the cylindrical phase becomes stable for $\lambda > 1.38$ and $f < 0.7$. Thus, it is observed that an imposed strain in the system can cause an apparent change in the phase boundary, i.e., the value of f between the bcc and cylindrical phases. (Strain cannot cause the same shift at the lamellar/cylindrical boundary.) However, in reality, this effect would be of negligible importance. This

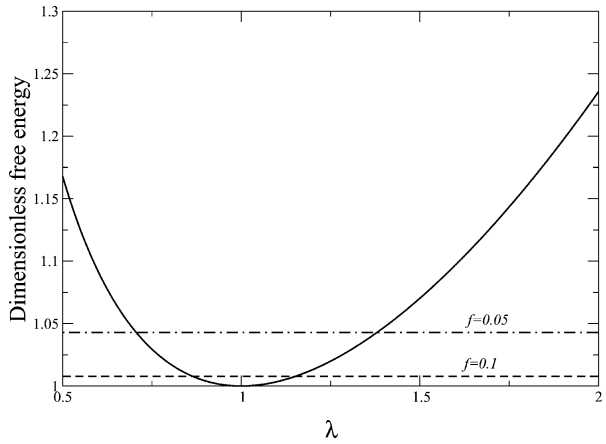

Figure 4. Dimensionless free energy (F/F_0) within the UCA as a function of strain. Solid curve is the bcc morphology, dashed curve is for the cylindrical morphology at $f = 0.1$ and dot−dashed curve is for the cylindrical morphology at $f = 0.05$.

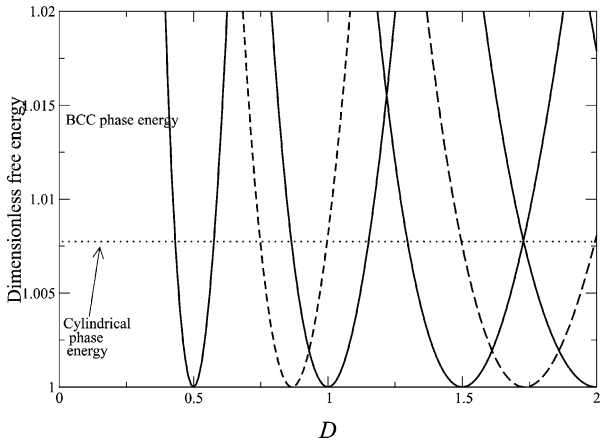

Figure 5. Dimensionless free energy (F/F_0) within the UCA as a function of scaled film thickness, $\mathscr{D}$, at $f = 0.1$. Solid curves are for layers of spheres where the strain direction lies along the edge of length h of the cube, dashed curves are for layers of spheres where the strain direction lies along the diagonal of the cube and the dotted curve is the cylindrical phase energy. When the bcc curves are below the cylindrical phase line, the bcc morphology should be observed. The following is a list of phases I predict to be observed on increasing the scaled thickness $\mathscr{D}$ from zero: vertical cylinders, half a layer of ellipsoids, vertical cylinders, half a layer of ellipsoids, one layer of ellipsoids, vertical cylinders, one and a half layers of ellipsoids, one layer of ellipsoids, two layers of ellipsoids.

is because in any bulk system one would never achieve such high strains as considered here.

3.1. Confined, Thin Films. One possibility of achieving comparably high strains, as considered here, is when block copolymer melts are confined to thin films,[3,4] usually by placing the melt between two, hard, flat plates. In this case, an imposed film thickness, D, is placed on the melt. This film thickness, in effect, imposes a strain on the melt because D is not necessarily an integer multiple of $h/2$ (the distance between two adjacent layers of spheres). Hence, the spheres will deform to ellipsoids and correspondingly the free energy, per chain, will rise. In fact, there are two possible orientations of the spheres when the bcc phase is placed in a thin film geometry (either along the [100] crystal axis or [111] crystal direction). The two orientations can be obtained from Figure 1. The first one, [100], is where the distance h between spheres aligns with film thickness and the second, [111], is where the diagonal (or distance $\sqrt{3}h/2$) between spheres aligns with the film thickness. If, for example, the film thickness D is close to an integer multiple of $h/2$, the first orientation will be preferable while, on the other hand, if D is close to an integer multiple of $\sqrt{3}h/2 \approx 0.87h$, the second orientation would be preferable. In this paper, I deal with the simplest case where the confining plates are chemically neutral with respect to each block and so neither of the A or B monomers would preferentially reside near these surfaces. This may be realized practically by coating the surfaces with random copolymers.[23] In fact, my analysis here would be relevant for plates which have slight preference for one monomer type over the other, as long as the bulk, i.e., bcc or cylindrical morphology, is not disrupted close to the confining plates. In the layer directly adjacent to the confining plates, the spheres must be half-spheres.[8,11]

In Figure 5, I plot the free energy of a thin film of the diblock melt at a minority block fraction of $f = 0.1$ as a function of scaled film thickness $\mathscr{D} \equiv D/h$ using the UCA. Our plot shows that the two orientations of the bcc phase have minimas at integer multiples of $^1/_2$ and $\sqrt{3}/2$. (The first (filled) bold curve with minima at $\mathscr{D} = {}^1/_2$ corresponds to half a layer of spheres, while the second bold curve with a minima at $\mathscr{D} = 1$ corresponds to one layer of spheres and so on.) At these points the bcc phase has perfectly spherical AB dividing surfaces. Away from these points, the imposed strain causes the free energy to rise. Once the strain is sufficiently far away from unity, the cylindrical phase becomes stable and the melt would be observed to have a cylindrical morphology with cylinders perpendicular to the confining plates. Note, it is for very small thicknesses that the cylindrical phase is prevalent. For larger thicknesses, the strain is not so large because more layers of spheres may be inserted to compensate for the imposed film thickness.

Recently, it has been realized that the cylindrical phase can be used to produce nanowires if the inner core phase is dissolved away and replaced by a suitable metal.[15] There is a limit to the radius of these nanowires because the radius of the cylinders is directly related to f (just as the radius of the spheres in the bcc phase is related to f, see the formula for R_{opt}, above). However, the present analysis shows there is a way to reduce the radii of the cylindrical phase to, theoretically, arbitrarily small radii by using the spherical phase and imposing an external strain on the spherical phase. If the film thickness of the confined melt is kept to a few layers, i.e., on the order of $h/2$, then the imposed strain will be large, and as a consequence, the cylindrical phase would have a lower free energy state and therefore should be observed. However, the length of the nanowires would be correspondingly small, which may not be desirable.

Experimentally it may be difficult to obtain such thin films or even control the film thickness accurately. In this case, I suggest it could be useful to use an electric field, perpendicular to the confining plates, to aid formation of arbitrarily small nanowires. It has been shown previously,[8,24] by theoretical methods, that a perpendicular electric field will aid alignment of the cylindrical phase if the dielectric permittivity of the minority phase ϵ_A is much larger than the dielectric permittivity of the majority phase ϵ_B. For example, the electrical energy, per chain, for the perpendicular orientation of the cylinders is $F_{\mathrm{elec}} = -{}^1/_2(f[\epsilon_A - \epsilon_B] + \epsilon_B)E^2Nv$. The electrical energy is proportional to the

square of the electric field, E. Note, F_{elec} is negative, which represents a lowering of the total free energy. If the morphology of the diblock melt is the bcc phase, the electrical energy is approximately $F_{elec} = -1/2\epsilon_B E^2 Nv$, since the majority phase almost entirely fills the volume between the confining plates. A slightly better estimate would be to account for the electrical energy due to the tiny A spheres as done for the cylindrical case by Ashok, Muthukumar, and Russell[24] and Pereira.[8] That is, the electrical energy of the cubic phase is $F_{elec} = -(1/2)\epsilon_B[1 - f((\epsilon_A - \epsilon_B)/(\epsilon_A + \epsilon_B))^2]E^2Nv$. The difference in electrical energy between perpendicular cylinders and spheres is ΔF_{elec} and is given by

$$\Delta F_{elec} = -\frac{1}{2}f\left[(\epsilon_A - \epsilon_B) + \epsilon_B\left(\frac{\epsilon_A - \epsilon_B}{\epsilon_A + \epsilon_B}\right)^2\right]E^2Nv \quad (12)$$

I note that the electrical energy difference is proportional to f, so that ΔF_{elec} dies off to zero as the minority block fraction diminishes. If $\epsilon_A \gg \epsilon_B$, this indicates the cylindrical phase may obtain a large advantage over the bcc phase. However, if $\epsilon_A < \epsilon_B$, the electrical energy would favor the bcc phase. If one looks at Figure 5, the above energies would simply represent a vertical shift of the bcc curves in comparison to the cylindrical energy by an amount of ΔF_{elec}. Thus, if one wants to use this method to obtain nanowires of arbitrarily small radii, one would need to ensure the minority type monomers (A monomers) have a higher dielectric permittivity in comparison to the majority monomer type. Finally, I note that the above electrical analysis is only qualitatively correct. The bcc phase electrical energy is only approximately correct. If one wants this energy more precisely, one would need to solve Maxwell's equations for a complex geometry, which would be an arduous task. The analysis also assumes the electric field is always perpendicular between the plates, an assumption which is not true near the edges. I also assume the electric fields which may be used are much smaller than the critical field which causes dielectric breakdown of the material. Despite all these assumptions, I believe that these results should be useful in practical situations.

As a practical comparison, I consider the sort of electric fields that would be required to obtain perpendicular orientation of cylinders for a melt which would, in equilibrium, be in the bcc morphology. If we look at Figure 5, which was calculated for a minority block fraction of 0.1, we can see that an additional electrical energy (measured in units of F_0), per chain, on the order of 0.01 would be necessary to induce stability of the cylindrical phase. For a minority fraction of 0.05, a similar plot tells us we would need an additional energy on the order of 0.05 to induce a cylindrical morphology. The electrical energy is given by eq 12 above, and so using experimental values from the literature we can estimate the size of the electrical field required to induce the cylindrical phase. I estimate that the center-to-center sphere distance is on the order of 100 nm, the surface tension is $\gamma_{AB} = 0.01$ J/m^2, and $\epsilon_A = 5 \times 10^{-11}$N/C while $\epsilon_B = 2 \times 10^{-11}$N/C. Substituting these values into (12), one estimates an electric field in excess of $E = 2.26 \times 10^7$N/C is needed to induce the cylindrical phase at $f = 0.1$, while a field of at least $E = 5.06 \times 10^7$N/C is needed at $f = 0.05$. For suitable materials, it is estimated[25,14] that dielectric breakdown occurs for fields in excess of 10^8N/C. Thus, it seems possible the present method may be useful for inducing the cylindrical morphology from the bcc phase.

4. Conclusions

The theoretical analysis in this paper has been carried out in the SSL ($\chi N \to \infty$). In this limit, the bcc (spherical) phase is expected to exist below $f \approx 0.12$. I have initially considered how the diblock melt deforms when put under a strain. I have shown that the spherical domains will deform anisotropically to either prolate spheroids (if the melt is under elongation) or oblate spheroids (if the melt is under compression). Although my theoretical methods are not exact, by estimating the free energy by two different methods, I can be fairly confident that the above predictions are valid. I have also estimated the bulk dilation and elliptic deformation constants for the melt.

I have shown that it is possible for the bcc morphology to revert to the cylindrical morphology if the strain in the system is significantly different to $\lambda = 1$. While this is expected to have negligible importance in bulk systems, where the strain would never be very different from unity, it would be expected to have much more significance for confined, thin films of the bcc phase. For extremely thin films, on the order of a layer of spheres or so, the cylindrical morphology is predicted. For thicker films the bcc phase should be observed, although the shape of the domains will be ellipsoidal. It has been shown that if one can use this method in conjunction with an applied electrical field perpendicular to the confining plates, it may be possible to induce the cylindrical phase, from an initial bcc melt, for much thicker films as well. One possible application of this work could be in producing nanowires, which have radii below the limit of the cylindrical phase. Of course there is a comparatively straightforward method of producing smaller radii nanowires. This is to use lower molecular weight polymers. In principle, one could use this in conjunction with an electric field and an initial spherical phase melt to obtain comparatively small (radii) nanowires.

Acknowledgment. I acknowledge the support of an ARC QEII Fellowship and assistance from J. R. May.

Appendix A. Ellipsoid Free Energy Calculation

In Appendix A, I give the steps to determining the free energy for an arbitrary ellipsoidal geometry within the UCA, starting from the Cartesian equation $x^2/l_x^2 + y^2/l_y^2 + z^2 = R^2$. The polar equation of the ellipsoid is then $r(\theta,\phi) = Rl\rho$ where

$$\rho = [1 - \beta\cos^2\theta + \cos^2\phi(l^2 - (1 - \beta\cos^2\theta))]^{-1/2} \quad (13)$$

and $\beta \equiv 1 - l_y^2/l_x^2$ and $l \equiv l_y$. Then the partial derivatives of ρ with respect to θ and ϕ are given by

$$\rho_\theta = -\beta\sin\theta\cos\theta\sin^2\phi\rho^3 \quad (14)$$

and

$$\rho_\phi = -\sin\phi\cos\phi[l^2 - (1 - \beta\cos^2\theta)]\rho^3 \quad (15)$$

If we define vector $\mathbf{t}$ by $\mathbf{t} \equiv \rho\cos\theta\sin\phi\mathbf{i} + \rho\sin\theta\sin\phi\mathbf{j} + \rho\cos\phi\mathbf{k}$, then the differential area element is given by $A_{\theta,\phi}\,d\theta\,d\phi$ where $A_{\theta,\phi} = R^2l^2|\mathbf{t}_\theta \times \mathbf{t}_\phi| = R^2l^2A'_{\theta,\phi}$.

Evaluating the cross-product appropriately one finds

$$A'_{\theta,\phi} = \{[(\rho_\theta \sin\phi \sin\theta + \rho \sin\phi \cos\theta)(\rho_\phi \cos\phi - \rho \sin\phi) - \rho_\theta \cos\phi(\rho_\phi \sin\phi \sin\theta + \rho \cos\phi \sin\theta)]^2 + [(\rho_\theta \sin\phi \cos\theta - \rho \sin\phi \sin\theta)(\rho_\phi \cos\phi - \rho \sin\phi) - \rho_\theta \cos\phi(\rho_\phi \sin\phi \cos\theta + \rho \cos\phi \cos\theta)]^2 + [(\rho_\theta \sin\phi \cos\theta - \rho \sin\phi \sin\theta)(\rho_\phi \sin\phi \sin\theta + \rho \cos\phi \sin\theta) - (\rho_\theta \sin\phi \sin\theta + \rho \sin\phi \cos\theta) \times (\rho_\phi \sin\phi \cos\theta + \rho \cos\phi \cos\theta)]^2\}^{1/2} \quad (16)$$

The angle between the normal to the surface of the ellipsoid at any point and the radius vector is denoted by η and is given by $\cos\eta = \nabla\Phi\cdot(\cos\theta \sin\phi\mathbf{i} + \sin\theta \sin\phi\mathbf{j} + \cos\phi\mathbf{k})/|\nabla\Phi|$, where $\Phi = x^2(1-\beta)/l^2 + y^2/l^2 + z^2$. Evaluating the derivatives and dot products, one finds

$$\cos\eta = \frac{\cos^2\theta \sin^2\phi(1-\beta)/l^2 + \sin^2\theta \sin^2\phi/l^2 + \cos^2\phi}{[\cos^2\theta \sin^2\phi(1-\beta)^2/l^4 + \sin^2\theta \sin^2\phi/l^4 + \cos^2\phi]^{1/2}} \quad (17)$$

The volume of the ellipsoid is $V_e = 4\pi R^3 l^2/[3(1-\beta)^{1/2}]$.

I may now evaluate the free energy for the ellipsoidal configuration as shown by Olmsted and Milner.[15] The total energy per chain F is a sum of AB interfacial energy, F_{AB} and elastic energy F_{el}, divided by the number of chains, which is $V_e/(N\nu)$. Thus, I find the free energy is

$$F = \frac{2}{3}F_0\lambda^{-1}(1-\beta)^{1/2}\frac{2}{\pi}\int_0^{\pi/2} d\theta\int_0^{\pi/2} A'_{\theta,\phi}\, d\phi + \frac{1}{3}F_0\lambda^2 l^3(1-\beta)^{1/2}\frac{2}{\pi}\int_0^{\pi/2} d\theta\int_0^{\pi/2}\rho^3 A'_{\theta,\phi}\cos\eta\, d\phi \quad (18)$$

The free energy is a function of three variables—λ, β, and l. For a particular strain, λ, one minimizes the energy over β and l. If the optimal relaxations in the orthogonal directions are the same, the optimal value of β is zero.

Appendix B. Free Energy Calculation for Anisotropic UCA Case

I now have the radius functions for my deformed geometry so, as in ref 15, I need the typical area element $A_{\theta,\phi}$ for the wedges. In the prolate spheroid case $A_{\theta,\phi} = R^2(1-e^2)\sin\phi[1-e^2(2-e^2)\cos^2\phi]^{1/2}/[1-e^2\cos^2\phi]^2$, while for the oblate spheroid the typical area element for a wedge is $A_{\theta,\phi} = R^2(1-e^2)^{-1}\sin\phi[1+\alpha^2(2+\alpha^2)\cos^2\phi]^{1/2}/[1+\alpha^2\cos^2\phi]^2$, where $\alpha^2 \equiv e^2/(1-e^2)$. According to ref 15, I can determine the interfacial energy of a typical wedge as $\gamma_{AB}\beta^2 A_{\theta,\phi}\, d\theta\, d\phi$. This yields, in the limit of $\delta\theta$, $\delta\phi \to 0$, for the prolate spheroid

$$F_{AB} = 4\pi R^2 f^{2/3}(1-e^2) \times \int_0^{\pi/2} d\phi \sin\phi \frac{[1-e^2(2-e^2)\cos^2\phi]^{1/2}}{[1-e^2\cos^2\phi]^2} \quad (19)$$

In the oblate spheroid case, I get

$$F_{AB} = 4\pi R^2 f^{2/3}(1-e^2)^{-1} \times \int_0^{\pi/2} d\phi \sin\phi \frac{[1+\alpha^2(2+\alpha^2)\cos^2\phi]^{1/2}}{[1+\alpha^2\cos^2\phi]^2} \quad (20)$$

The elastic energy is more difficult than in the spherically symmetric case because one must get the perpendicular projection of the area element onto the radius vector.[15] Consider a point $r(\theta,\phi)$ on the ellipsoid surface. The tangent plane to this point makes an angle ψ with a horizontal plane (i.e., a plane orthogonal to strain direction). Then the angle between the tangent plane and the normal plane to the radius vector is η and given by $\eta = \pi - (\psi + \phi)$. The projection of the area element, at the point on the surface $r(\theta,\phi)$, on to the normal plane is then $A^*_{\theta,\phi} = \cos\eta A_{\theta,\phi}$. It can be shown that $\tan\psi = -\tan\phi/(1-e^2)$ and so the projection is $A^*_{\theta,\phi} = R^2 \sin\phi/[1-e^2\cos^2\phi]$. (In the oblate spheroid case, the projected area is $A^*_{\theta,\phi} = R^2 \sin\phi/[1+\alpha^2\cos^2\phi]$.) Thus, the stretching energy in the A and B domains can be determined using (1) and summing over the prolate spheroid

$$F_{el} = \frac{k_B T}{48 N\nu}\frac{\pi^2}{Na^2}\left[\frac{1}{10f^{1/3}} + \frac{(1-f^{1/3})^3(f^{2/3}+3f^{1/3}+6)}{10(1-f)^2}\right]4\pi R^5(1-e^2)^{3/2}\int_0^{\pi/2}\frac{\sin\phi\, d\phi}{[1-e^2\cos^2\phi]^{5/2}} \quad (21)$$

The elastic energy in the oblate spheroid case is

$$F_{el} = \frac{k_B T}{48 N\nu}\frac{\pi^2}{Na^2}\left[\frac{1}{10f^{1/3}} + \frac{(1-f^{1/3})^3(f^{2/3}+3f^{1/3}+6)}{10(1-f)^2}\right]4\pi R^5(1-e^2)^{-3/2}\int_0^{\pi/2}\frac{\sin\phi\, d\phi}{[1+\alpha^2\cos^2\phi]^{5/2}} \quad (22)$$

The sum of the wedge volumes must equal the volume of an ellipsoid which, in this case, is just $V = 4\pi l^2 R^3/3 = 4\pi R^3(1-e^2)/3$, for a prolate spheroid, and for an oblate spheroid $V = 4\pi R^3/3(1-e^2)$.

Appendix C. Free Energy Calculation for Isotropic SPA Case

In this case one can show the side length of the square faces, which I denote as b, are related to h by $b^2 = h^2/8$. The side lengths of the hexagonal faces are also b. The line joining the center of the cube to each of the 8 corners has length $\sqrt{3}h/2$, and this line is normal to the hexagonal faces and passes through the center of the hexagons. The distance from the center of the cube to a hexagonal face is $\sqrt{3}h/4$. I now focus on a $^1/_8$ corner section cube of side length $h/2$, since all other sections are the same. It consists of three, $^1/_4$ square faces and one hexagonal face. For the square faces, the radius and area element can be shown to be just $r(\theta,\phi) = (h/2)\sec\theta \sec\phi$ and $A_{\theta,\phi} = (h^2/4)\sec^2\theta \sec^2\phi$. Assume the z-axis passes through the center of the square face with x-axis going along horizontal and y-axis along vertical. The area integrated over, then, is the triangle bounded by $x = 0$, $y = 0$ and $y = b/\sqrt{2} - x$. The perpendicular distance from the origin to the square face is $h/2$, so that converting x and y to polar coordinates one finds $x = (h/2)\tan\theta$ and $y = (h/2)\tan\phi$. Thus, the AB interfacial energy for this triangle ($^1/_4$ of the square face) is $F^i_{AB} =$

$\gamma_{AB}f^{2/3}(h^2/4)\int_0^{\arctan((2)^{1/2}b/h)} d\phi \int_0^{\arctan((2)^{1/2}b/h-\tan\phi)} d\theta \sec^2\theta \sec^2\phi$ which yields $F_{AB}^{i} = \gamma_{AB}f^{2/3}b^2/4$. The elastic stretching energy is determined using (1), with the additional proviso that A_{wedge} must be the perpendicular projection of the area element onto the radius vector. The radius $r(\theta,\phi)$ and area element $A_{\theta,\phi}$ are given above for each wedge and, to obtain the perpendicular projection of each area element, I multiply $A_{\theta,\phi}$ by $\cos\theta\cos\phi$. Doing this, in conjunction with (1), one obtains

$$F_{el}^{i} = \frac{k_BT}{48Nv}\frac{\pi^2}{Na^2}\left[\frac{1}{10f^{1/3}} + \frac{(1-f^{1/3})^3(f^{2/3}+3f^{1/3}+6)}{10(1-f)^2}\right]\left(\frac{h}{2}\right)^5 I_i \quad (23)$$

where $I_i = \int_0^{\arctan((2)^{1/2}b/h)} d\phi \int_0^{\arctan((2)^{1/2}b/h-\tan\phi)} d\theta \sec^4\theta\sec^4\phi$. Evaluating I_i one gets $I_i = 1561/11520$. The corresponding volume for this triangle is just $V^i = hb^2/24$. As there is a triangle on each of the three square faces, one must multiply all of these energies and volumes by a factor of 3. Next I consider the slanted hexagonal face, which has six equal sides of length b. I now assume that the Cartesian axis system used has its origin at the center of the cube and is aligned such that the z-axis is along the perpendicular to the slanted face. As a consequence, it also passes through the center of the hexagon. The x-axis then runs through a corner of the hexagon and the y axis through the center of one of the hexagon's edges. See Figure 2a. The radius and area element for this slanted face are $r(\theta,\phi) = d\sec\theta\sec\phi$, where $d = \sqrt{3}h/4$ and $A_{\theta,\phi} = d^2\sec^2\theta\sec^2\phi$. The interfacial and elastic energies follow as above, except the boundaries for the integrals differ since I am integrating over a hexagonal shape. Consider a quarter of the hexagon bounded by $x = 0$, $y = 0$, $y = \sqrt{3}b/2$, and $y = \sqrt{3}(b-x)$. All other quarters are exactly the same. Thus, the interfacial energy for the entire hexagonal slanted face is $F_{AB}^{ii} = 4\gamma_{AB}f^{2/3}d2\int_0^{\arctan[(3)^{1/2}b/(2d)]} d\phi \int_0^{\arctan(b/d-\tan\phi/(3)^{1/2})} d\theta \sec^2\theta\sec^2\phi$, which yields $F_{AB}^{ii} = \gamma_{AB}f^{2/3}3\sqrt{3}b^2/2$. The stretching energy is

$$F_{el}^{ii} = \frac{k_BT}{48Nv}\frac{\pi^2}{Na^2}\left[\frac{1}{10f^{1/3}} + \frac{(1-f^{1/3})^3(f^{2/3}+3f^{1/3}+6)}{10(1-f)^2}\right]\left(\frac{h}{2}\right)^5 \times (9\sqrt{3}/8)I_{ii} \quad (24)$$

where $I_{ii} = \int_0^{\arctan[(3)^{1/2}b/(2d)]} d\phi \int_0^{\arctan(b/d-\tan\phi/(3)^{1/2})} d\theta \sec^4\theta\sec^4\phi$. (Note that $2d/h = \sqrt{3}/2$.) Evaluating I_{ii} one gets $I_{ii} = 697\sqrt{3}/2160$. The volume corresponding to the hexagonal face is $V^{ii} = \sqrt{3}b^{2d/2.}$

I now have all the elements to calculate the free energy of the bcc phase in the SPA. I thus have $F_{spa} = Nv(3F_{AB}^{i} + 3F_{el}^{i} + F_{AB}^{ii} + F_{el}^{ii})/(3V^i + V^{ii})$. The denominator is just $(h/2)^3/2$. Thus, the total energy per chain is $F_{spa} = (\square/(h/2))(1/2 + \sqrt{3})1/2 + \bigcirc((h/2))^2(1561/5760 + 697/960)$. Minimizing this energy with respect to h one finds the optimal h is given by $(h/2)_{opt} = R_{opt}[(1/2 + \sqrt{3})/(5743/2880)]^{1/3}$ and the minimum free energy,[17] $\bar{F}_{spa}$, is $\bar{F}_{spa} = F_0(1/2 + \sqrt{3})^{2/3}(5743/23040)^{1/3}$.

Appendix D. Free Energy for Anisotropic SPA Case

For the rhombus faces, the length in the strain direction of the rhombus (along one diagonal of the rhombus) is $b/\sqrt{2}$, while in the orthogonal direction (along other diagonal), the length is $lb/\sqrt{2}$. See Figure 2b. Thus, the side length of the rhombus is $b\sqrt{(l^2+1)/2}$ and the obtuse angle, ζ, is given by $\zeta = 2\arctan(l^{-1})$. The triangle I integrate over is bounded by $x = 0$, $y = 0$ and $y = (b/\sqrt{2} - x/l)$. Our radius and area elements are $r(\theta,\phi) = (lh/2)\sec\theta\sec\phi$ and $A_{\theta,\phi} = (lh/2)^2\sec^2\theta\sec^2\phi$. The AB interfacial energy therefore becomes, for this section, $F_{AB}^{i} = \gamma_{AB}f^{2/3}((lh/2))^2\int_0^{\phi_0} d\phi \int_0^{\theta(\phi)} d\theta \sec^2\theta\sec^2\phi$, where $\theta(\phi) = \arctan(1/2 - l\tan\phi)$ and $\phi_0 = \arctan(2l)^{-1}$. Completing the integral, one obtains $F_{AB}^{i} = \gamma_{AB}f^{2/3}h^2l/(32)$. The elastic stretching energy follows as in the isotropic case except the boundary for the integration domain differs slightly. So F_{el}^{i} is given by (23), but with $I_i = l^5\int_0^{\phi_0} d\phi \int_0^{\theta(\phi)} d\theta \sec^4\theta\sec^4\phi$. The result for the integral is given in Appendix E. Finally, the volume corresponding to this region is $V^i = h^3l^2/192$.

The second part of the free energy calculation is the slanted (anisotropic) hexagonal face. In the isotropic case, the origin for the coordinate system was the center of the cube, and I aligned the z-axis of the coordinate system used with the normal to the slanted face. This also happened to be along the line joining the center of the cube to the corner and through the center of the hexagonal face. In the anisotropic case, I define the origin of the coordinate system used to be the center of the cuboid. Then the z-axis is again defined to be perpendicular to the slanted hexagonal face. However, it is not aligned with the vector from the center of the cuboid to the corner and does not go through the center of the hexagon. Instead the intersection with the hexagonal face occurs at a point which is g units from the bottom edge of the hexagon. See Figure 2c. Recall that the shortest distance from the center of the cuboid to a face which is perpendicular to the strain direction is $h/2$, and the shortest distance to the other (sides) is $lh/2$. Thus, the angle the perpendicular to the slanted hexagonal face makes with the plane orthogonal to the strain direction is ν and given by $\tan\nu = l/\sqrt{2}$. The perpendicular distance from the origin to the slanted hexagonal face is d and given by $d = 3lh/4L$ where $L \equiv \sqrt{l^2+2}$. The side lengths of the hexagons are lb and $b\sqrt{(l^2+1)/2}$ (Figure 2c) and $g = 3l^2h/(4\sqrt{2}L)$.

The radius and area elements are (following the isotropic case) $r(\theta,\phi) = d\sec\theta\sec\phi$ and $A_{\theta,\phi} = d^2\sec^2\theta\sec^2\phi$. The interfacial energy for this face is

$$F_{AB}^{ii} = 2\gamma_{AB}f^{2/3}d^2[\int_{\phi l}^{\phi m} d\phi \int_0^{\theta_l(\phi)} d\theta \sec^2\theta\sec^2\phi + \int_{\phi m}^{\phi u} d\phi\int_0^{\theta u(\phi)} d\theta \sec^2\theta\sec^2\phi] \quad (25)$$

Here the terminals are given by $\phi_l = \arctan(-g/d)$, $\phi_m = \arctan[(bL/2 - g)/d]$, $\phi_u = \arctan[(bL - g)/d]$, $\theta_l(\phi) = \arctan[l(bL/2 + g)/(Ld) + l\tan\phi/L]$ and $\theta_u(\phi) = \arctan[l(3bL/2 - g)/(Ld) - l\tan\phi/L]$. Completing all the necessary integrals one finds $F_{AB}^{ii} = \gamma_{AB}f^{2/3}3h^2Ll/16$. The elastic energy follows the isotropic case, with a slightly different domain to integrate over. Thus, F_{el}^{ii} is given by (24) with I_{ii} given by $I_{ii} = [3^5l^5/2^4L^5]\int_{\phi l}^{\phi m} d\phi \int_0^{\theta l(\phi)} d\theta \sec^4\theta\sec^4\phi + \int_{\phi m}^{\phi u} d\phi \int_0{}^{\theta u(\phi)} d\theta \sec^4\theta\sec^4\phi]$.

The integrals are cumbersome to write and are given in Appendix E. Finally, the volume for this face is $V^{ii} = 3h^3l^2/64$.

The final face to complete is the square face on the surface of the cuboid, which is perpendicular to the strain direction. See Figure 2d. For this face, I integrate over a domain which is a factor l times larger in both directions than in the isotropic case. Thus, the interfacial AB energy is given by $F_{AB}^{iii} = \gamma_{AB} f^{2/3}((h/2))^2 \int_0^{\phi t} d\phi \int_0^{\theta t(\phi)} d\theta \sec^2\theta \sec^2\phi$, where $\phi_t = \arctan[l/(2)]$ and $\theta_t(\phi) = l/2 - \tan\phi$. Completing the integral I get $F_{AB}^{iii} = \gamma_{AB} f^{2/3} l^2 h^2/32$. The elastic energy is given by (23) with I_i replaced by (here I shall call it I_{iii} to denote the third part of the free energy calculation) $I_{iii} = \int_0^{\phi t} d\phi \int_0^{\theta t(\phi)} d\theta \sec^2\theta \sec^2\phi$. Once again this is evaluated in Appendix E. The volume corresponding to this face is $V^{iii} = l^2h^3/192$.

I have all the components for the free energy in the anisotropic case using the SPA. Thus, the total energy per chain is $F_{spa} = Nv(2F_{AB}^{i} + 2F_{el}^{i} + F_{AB}^{ii} + F_{el}^{ii} + F_{AB}^{iii} + F_{el}^{iii})/(2V^{i} + V^{ii} + V^{iii})$.

Appendix E. Elastic Integrals for Anisotropic SPA Calulation

The integrals I_i, I_{ii}, and I_{iii} for the elastic energies in the anisotropic SPA calculation are calculated to be as follows:

$$I_i = \frac{25l^4}{192} + \frac{61l^2}{11520} \tag{26}$$

$$\begin{aligned} I_{ii} = {} & \left(\frac{3^5l^5}{2^4L^5}\right)\left[\frac{l}{2L}(1+\omega^2){x_m}^2 - \frac{2l\omega}{3L}{x_m}^3 + \left(\frac{l}{L} + (1+\omega^2)\frac{l^3}{3L^3}\right)\frac{{x_m}^4}{4} - \frac{2\omega l^3}{15L^3}{x_m}^5 + \frac{l^3}{18L^3}{x_m}^6\right] - \\ & \left(\frac{3^5l^5}{2^4L^5}\right)\left[\frac{l}{2L}(1+\omega^2){x_l}^2 - \frac{2l\omega}{3L}{x_l}^3 + \left(\frac{l}{L} + (1+\omega^2)\frac{l^3}{3L^3}\right)\frac{{x_l}^4}{4} - \frac{2\omega l^3}{15L^3}{x_l}^5 + \frac{l^3}{18L^3}{x_l}^6\right] - \\ & \left(\frac{3^5l^5}{2^4L^5}\right)\left[\frac{l}{2L}(1+\mu^2){x_l}^2 - \frac{2l\mu}{3L}{x_l}^3 + \left(\frac{l}{L} + (1+\mu^2)\frac{l^3}{3L^3}\right)\frac{{x_l}^4}{4} - \frac{2\mu l^3}{15L^3}{x_l}^5 + \frac{l^3}{18L^3}{x_l}^6\right] + \\ & \left(\frac{3^5l^5}{2^4L^5}\right)\left[\frac{l}{2L}(1+\mu^2){x_m}^2 - \frac{2l\mu}{3L}{x_m}^3 + \left(\frac{l}{L} + (1+\mu^2)\frac{l^3}{3L^3}\right)\frac{{x_m}^4}{4} - \frac{2\mu l^3}{15L^3}{x_m}^5 + \frac{l^3}{18L^3}{x_m}^6\right] \end{aligned} \tag{27}$$

where $\omega = L^2/(3\sqrt{2}l) + l/\sqrt{2}$, $\mu = L^2/(\sqrt{2}l) - l/\sqrt{2}$, $x_l = L^2/(3\sqrt{2}l)$, and $x_m = 2L^2/(3\sqrt{2}l)$, and finally

$$I_{iii} = \frac{l^6}{11520} + \frac{l^4}{96} + \frac{l^2}{8} \tag{28}$$

References and Notes

(1) Bates, F. S.; Fredrickson, G. H. *Physics Today* **1999**, *52*, 32.
(2) Bates, F. S.; Fredrickson, G. H. *Annu. Rev. Phys. Chem.* **1990**, *41*, 525. Bates, F. S.; Fredrickson, G. H. *Annu. Rev. Mater. Sci.* **1996**, *26*, 501.
(3) Fasolka, M. J.; Mayes, A. M. *Annu. Rev. Mater. Res.* **2001**, *31*, 323.
(4) Chakraborty, A. K.; Golumbfskie, A. J. *Annu. Rev. Phys. Chem.* **2001**, *50*, 537.
(5) Turner, M. S.; Rubenstein, M.; Marques, C. M. *Macromolecules* **1994**, *27*, 4986.
(6) Huinink, H. P.; Brokken-Zijp, J. C. M.; van Dijk, M. A. *J. Chem. Phys.* **2000**, *112*, 2452.
(7) Pereira, G. G. *Phys. Rev. E* **2001**, *63*, 061809.
(8) Pereira, G. G. *Eur. Phys. J. E* **2002**, *7*, 273.
(9) Pereira, G. G. *J. Chem. Phys.* **2002**, *117*, 1878.
(10) Wang, Q.; Nealey, P. F.; de Pablo, J. J. *Macromolecules* **2001**, *34*, 3458.
(11) Chen, H. Y.; Fredrickson, G. H. *J. Chem. Phys.* **2002**, *116*, 1137.
(12) Tyler, C. A.; Morse, D. C. *Macromolecules* **2003**, *36*, 3764.
(13) Park, C.; Simmons, S.; Fetters, L. J.; Hsiao, B.; Yeh, F.; Thomas, E. L. *Polymer* **2000**, *41*, 2971.
(14) Tsori, Y.; Tournilhac, F.; Andelman, D.; Leibler, L. *Phys. Rev. Lett.* **2003**, *90*, 145504.
(15) Thurn-Albrecht, T.; Schotter, J.; Kastle, G. A.; Emley, N.; Shibauchi, T.; Krusin-Elbaum, L.; Guarini, K.; Black, C. T.; Tuominen, M. T.; Russell, T. P. *Science* **2000**, *290*, 2126.
(16) Walheim, S.; Schaffer, E.; Mlynek, J.; Steiner, U. *Science* **1999**, *283*, 520.
(17) Semenov, A. N. *Sov. Phys. JETP (Engl. Transl.)* **1985**, *61*, 733. Semenov, A. N. *Zh. Eksp. Teor. Fiz.* **1985**, *88*, 1242.
(18) Olmsted, P. D.; Milner, S. T. *Macromolecules* **1998**, *31*, 4011.
(19) de Gennes, P. G.; Prost, J. *The Physics of Liquid Crystals*; Clarendon Press: Oxford, England, 1993.
(20) Hyde, S. T. in *Handbook of Applied Surface and Colloid Chemistry*; Holmberg, K., Ed.; John Wiley & Sons: New York, 2001.
(21) This energy is slightly different to Olmsted and Milner.[18] They get an $\bar{F}_{spa} \approx 1.072F_0$, while here I obtain $\bar{F}_{spa} \approx 1.0749F_0$. Note that this free energy is still less than Olmsted and Milner's face-centered cubic (fcc) estimate, indicating the bcc phase is still the most favorable packing arrangement for the spherical phase according to the SPA.
(22) Matsen, M. W.; Bates, F. S. *Macromolecules* **1006**, *29*, 7641.
(23) Mansky, P.; Liu, Y.; Huang, E.; Russell, T. P.; Hawker, C. *Science* **1997**, *275*, 1458.
(24) Ashok, B.; Muthukumar, M.; Russell, T. P. *J. Chem. Phys.* **2001**, *115*, 1559.
(25) *User's Practical Selection Handbook for Optimum Plastics, Rubbers and Adhesives*; The International Technical Information Institute: Tokyo, Japan, 1976.
(26) I use for the bulk modulus $B = (K_{11} + 2K_{12})/3$ and $C = K_{12}$. Note, there seems to be a misprint in the paper of Tyler and Morse for the bulk modulus, where they multipy by a factor of 3 rather than divide. For verification, see p 290 of: Marder, M. P. *Condens. Matter Physics*; John Wiley & Sons: New York, 2000.

MA030052J